Cement and Concrete Research 40 (2010) 1471–1487

Contents lists available at ScienceDirect

Cement and Concrete Research

journal homepage: http://ees.elsevier.com/CEMCON/default.asp

Predicting the pullout response of inclined hooked steel fibers

F. Laranjeira *, C. Molins, A. Aguado

Department of Construction Engineering, Universitat Politècnica de Catalunya UPC, Edifici C1, Campus Nord UPC, Jordi Girona 1-3, 08034 Barcelona, Spain

ARTICLE INFO

Article history:
Received 20 October 2009
Accepted 18 May 2010

Keywords:
Pullout strength (C)
Tensile properties (C)
Fiber reinforcement (E)
Orientation

ABSTRACT

Steel fiber reinforced concrete (SFRC) is symptomatically an anisotropic material due to the random orientation of fibers within the cement matrix. Fibers under different inclination angles provide different strength contributions at a given crack width. Therefore the pullout response of inclined fibers is a paramount subject to understand and quantify SFRC behavior, particularly in the case of fibers with hooked ends, which are currently the most widely used. Several experimental results were considered to validate the approach and to assure its suitability on distinct material properties and boundary conditions. The good agreement on predicting the pullout behavior of these fibers encourages its use towards a new concept of design and optimization of SFRC.

1. Introduction

The last four decades have seen a large number of research studies on fiber reinforced concrete, most of which devoted to steel fibers [1]. Among various attempts to improve bond-slip characteristics the most effective is mechanical deforming [2]. Thereby it is not surprising that almost all commercially available fibers at present are mechanically deformed [2] and that they have been conceived and introduced in the market over thirty years ago [1]. However, most of bond-slip investigations focused primarily on fibers without deformations (straight fibers) and therefore scarce knowledge on behavior of deformed fibers led to commercial geometries which were only "intuitive" [2].

To understand the effects of fiber geometry on the mechanical behavior of SFRC pullout tests on aligned fibers have been extensively carried out during the years [3]. Nonetheless mechanisms associated with pullout behavior of deformed fibers are not well understood [4] and, apart from experimental observations, few models attempted to account for the mechanical deformation [5–8].

Modeling the effect of the hook on steel fibers was advanced by Van Gysel [5] by assuming that hook geometry is a sum of straight and curved segments. Using the principle of energy conservation advanced by Chanvillard [6] the procedure is based both on theoretical and experimental considerations and accounts for fiber debonding, plastic deformations and additional frictional forces due to incomplete straightening of the hook. An alternative approach was proposed by Alwan et al. [7] using the concept of a frictional pulley along with two plastic hinges to simulate the hook action. The model consists of a two-step procedure and considers the contribution of two hinges at the first stage and one hinge superposition accounting for frictional and mechanical components. Subsequently a new model based on the concept of non-linear springs to resemble the effect of the hook was advanced by Sujivorakul et al. [8]. Applying an iterative procedure over the geometry of the mechanical anchorage, the approach superposes the effect of the spring on previous pullout models for straight fibers [9].

Despite the valuable understanding provided by the aforementioned models, their focus relies on the strengthening contribution provided by the hook on the pullout of aligned fibers. Nonetheless further complications arise when fibers lay under a certain inclination angle respect to load direction and the stress field in the vicinity of fiber becomes highly complex, as occur in actual composite [2].

Research on the pullout response of inclined fibers with hooked ends has been performed mostly on experimental basis. Likewise extensive works investigated the influence of fiber inclination angle [2,4,5,10,11] and embedded length [4,5,11] on the pullout behavior. In some experiments different strengths of cementitious matrices [2,4,5] and fiber yield strengths were applied [5] and the influence of the hook was evaluated by comparing pullout responses with the ones of straight fibers [3,11]. Although these procedures allow an effective quantification of differences on pullout behavior with varying parameters, they are restricted to a set of experimental boundary conditions and material properties. Their capacity on providing an effective understanding of the pullout mechanisms is very limited and justifies why no model has been able to fully explain what actually happens at the critical cracked section in terms of fiber–matrix interactions [12]. Regarding that fiber pullout is the major mechanism contributing to toughness of SFRC [13] a proper prediction on the pullout behavior of inclined fibers is of the utmost importance for composite design and tailoring.

* Corresponding author. Tel.: +34 34934017347; fax: +34 34934054135.
E-mail addresses: filipe.laranjeira@upc.edu (F. Laranjeira), climent.molins@upc.edu (C. Molins), antonio.aguado@upc.edu (A. Aguado).

0008-8846/$ – see front matter © 2010 Elsevier Ltd. All rights reserved.
doi:10.1016/j.cemconres.2010.05.005

A model for the pullout response of inclined straight fibers was advanced in a previous paper [14]. Such model is herein extended to fibers with hooked ends which, up to the present, represent the most widely used steel fibers' geometries used on concrete reinforcement. A description of the pullout response of this type of fibers is firstly presented. Following, a new conceptual approach to predict their pullout behavior is introduced on a comparative manner regarding the one previously advanced for straight fibers. The model is then validated against several experimental pullout tests from literature.

2. Research significance

Mechanical deformation of fibers introduces additional complexity on the pullout response of inclined fibers. Although fibers with hooked ends have been largely investigated, predicting their load-crack width relationships under any inclination angle has not yet been solved. This paper proposes a new analytical model to predict such pullout response within a straightforward method, taking as input parameters properties of constituent materials and pullout tests of fibers aligned with load direction. Model validation is performed through published experimental data in which large variety of fibers and matrices were used within different boundary conditions. Results show that this approach provides a powerful tool to develop a conceptual, comprehensive and design-oriented constitutive model for the tensile behavior of SFRC.

3. Pullout behavior

3.1. Main concepts

The pullout behavior of hooked fibers comprises all the phenomena described for inclined straight fibers such as fiber debonding, matrix spalling, frictional sliding and fiber removal. Nonetheless hooked ends imply plastic deformations which increase the force required to pullout the fiber, thus magnifying the matrix spalling effects of inclined fibers.

To account for the contribution provided by the hook along fiber slippage, a clear physical comprehension of its straightening process is required. Correlations between fiber pullout and respective load-crack width responses were advanced by Pompo et al. [15] through video photography techniques. From that research a typical pullout response of inclined fibers was suggested, consisting of four distinct regions: (1) elastic response followed by debonding; (2) fiber pullout and straightening processes; (3) frictional sliding within the straight matrix duct; and (4) fiber removal from the matrix. Such trend resembles the typical pullout behavior considered for straight fibers [14] with exception of stage concerning fiber straightening (region 2) which was absent in straight fibers and, consequently, will now be discussed with detail.

3.2. Correlation between geometry of the hook and pullout response

The correlation between fiber pullout responses and the several deformation phases of the hook requires accurate measurements of its geometry. According to investigations on steel fibers with diameters of 0.50 and 0.80 mm [5], the hook's geometry was found to be composed of straight and arc segments (Fig. 1). Considering the reported magnitude for the radius of curvature (about 1.20 mm) each arc-length was approximately 1.05 mm whereas intermediate straight segments were about 1.45 and 1.20 mm (total hook length of 4.75 mm).

The region of pullout response concerning fiber straightening comprises four main stages (Fig. 2). The crack widths (w) and the increments of crack width (Δw) at each of these stages are suggested in Fig. 2 according to the hook's geometry advanced in Fig. 1.

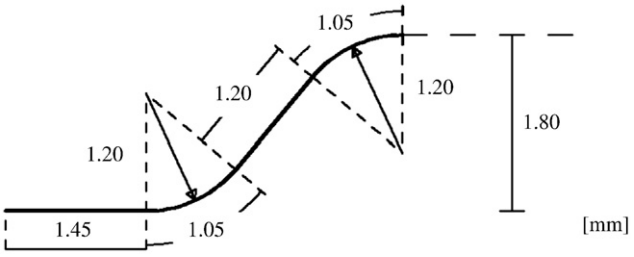

Fig. 1. Geometry of fiber hooked-end according to dimensions reported by [5].

At the beginning of the pullout process fiber has just been fully debonded and therefore its end section (G_1 in Fig. 2a) as well as the intermediate sections of the arc lengths (G_2 and G_3 in Fig. 2a) coincides with the initial print of the hook. Then both curved sections are progressively subjected to bending and plastic deformations, leading to a substantial increase on the pullout load. The maximum force required to pullout the fiber arises when G_2 and G_3 enter the straight segments of the matrix duct walls, which occurs for fiber slippages of about half of the arcs length (Fig. 2b).

Afterwards pullout load decreases given that G_2 and G_3 do not undergo significant plastic deformations while slipping along the straight ducts. However, once G_1 passes through the original print of section G_2, the latter is already at the next curved length of the hook print where it is forced to bend contrarily to its original shape. Considering the relative slippages at which G_1 and G_2 experiment maximum plastic deformations (1.48 and 1.72, respectively), pullout load may stabilize for an increment of crack width of about 1.60 mm (Fig. 2c).

At the third stage of hook deformation a moderate decrease in pullout load occurs due to the entrance of G_2 on the last straight segment of the duct. The pullout load is now mainly governed by the local friction effects imposed by G_1 and G_3 along the duct walls, thus keeping the pullout load nearly stable. When G_1 enters the second curved segment, abrasion against the duct walls increases due to incomplete straightening of the last straight portion (Fig. 2d). The final stage of the straightening process occurs when G_1 enters the straight duct (Fig. 2e). At this instant, although no further plastic deformations occur on the fiber, a residual resistance is prone to remain due to incomplete straightening of the hook. Likewise the hook slips along the ducts with a three-point contact mechanism [15] which can be clearly identified by comparing the hook's geometries before and after testing (Fig. 3), as also pointed out by other researchers [3].

3.3. Aligned fibers

The magnitude of the contribution provided by the mechanical anchorage depends upon several material properties. The larger the fiber diameter, the more energy has to be invested to deform the fiber due to its increasing bending stiffness [5]. Pullout tests on aligned fibers reported that maximum loads increase less than proportionally with fiber squared diameter, under similar pullout conditions and geometry of the hooked ends [5].

Similarly to straight fibers, the pullout performance has also been shown to be enhanced by improving the properties of the matrix in which fibers are embedded [3,5]. Experiments on steel fibers with 1200 MPa tensile yield strength reported 25% increment on maximum loads when testing fibers from normal to high strength matrices ($f_{cm}=47$ MPa and $f_{cm}=76$ MPa) whereas larger increments (about 65%) were observed when using fibers with 2100 MPa tensile yield strength [5].

Since the peak load is controlled by the plastic deformations of the hooks, an alternative and more effective method to improve pullout performance consists on increasing fibers tensile strength. The

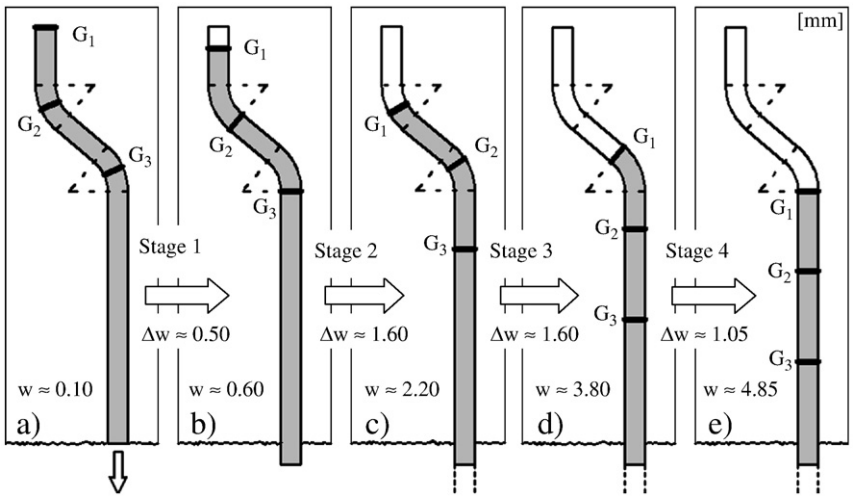

Fig. 2. Main stages of the straightening process of the hooked-end within the cement matrix.

investigation performed by Van Gysel [5] denoted an increment of 100% on the peak load when improving the tensile yield strength of fibers from 1200 to 2100 MPa on high strength matrices (f_{cm} = 76 MPa). A smaller increment was found (50%) when such improvement was performed on normal strength matrices (f_{cm} = 47 MPa), inducing that lower bond strength conditions might not have allowed full straightening of the hooked ends.

A commitment between matrix composition and fiber tensile strength shall be pursued in order to extract the maximum performance while avoiding brittle failure of the fibers. How to optimize these material properties will be further addressed in Section 5.

3.4. Inclined fibers

3.4.1. Experimental observations

Tests on inclined fibers showed that crack widths at peak increase with the inclination angles [2,4,5,10,11] and those were found to be generally independent of fiber embedded length providing that the hook-end was fully mobilized [4]. These increments of crack width are most likely a combination of fiber straightening with crushing and spalling of the concrete that take place at the corner where fiber enters the matrix [2,4,11,16] (Fig. 4). At large inclination angles the pullout response becomes progressively less influenced by the matrix strength and increasingly governed by the mechanical properties of the fiber as it attempts to straighten in line with the loading direction [4].

Optimum peak loads of hooked fibers occur under non-zero inclination angles due to the increasing friction that occur at fiber exit point. Experiments indicate that optimal fiber inclinations angles may be within 10°–30° [2,4,10] with increments at peak load with respect to aligned fibers up to 20% [4]. The latter are sometimes limited by fiber rupture, which introduces a brittle and undesirable failure mode. Hence two major pullout failure modes may occur, either by straightening and removal of the fiber or, alternatively, by fiber rupture [2,4,5,11,17].

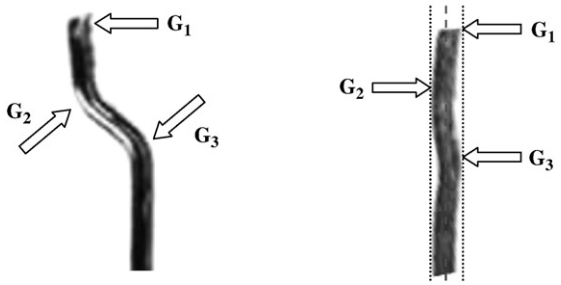

Fig. 3. Detail of hook geometry before testing (left) and after pullout (right).

Experimental works [2,4,5,10,11,16] showed that the load at which fibers fail decreases at increasing inclination angles. The reduction in the ultimate load may be best explained by Bartos and Duris [16] who introduced a new fiber characteristic, the so-called inclined tensile strength, which accounts for the coupled nature of axial, bending and shear stresses that occur at the fiber exit point.

Fiber rupture takes place during the early stage of the pullout process where relative slippage is still being greatly counteracted by the hook. Therefore the maximum curvature nearby fiber exit point is limited to a short extent of the fiber that can be idealized as a single plastic hinge. For fibers under large inclination angles the axial component of the pullout mechanism is not dominant and rupture tends to occur due to attainment of the ultimate strain capacity of the steel at the exit point from the matrix. Although this is the most commonly observed location for fiber rupture [2,5,11], fracture at the hook portion has also been observed [4]. This may occur due to the small distance between the actual fiber exit point and the portion where the hook is located, typically when matrix spalling produces small fiber embedded lengths. In those cases bending stresses generated by local curvature extend towards inner sections of the fiber on a degree dependent upon type of fiber, shape, flexibility and angle [18]. Hence rupture at the hook portion occurs as result of the superposition of bending stresses with the ones existing from the straightening process.

Regarding the severe decrease of the total pullout energy caused by fiber rupture, the consideration of an inclined tensile strength rather than the co-axial one is fundamental to evaluate pullout of inclined fibers appropriately [16].

3.4.2. Interpretation of the pullout response

Taking into account the aforementioned concepts and the trends of experimental results reported in literature, eight key-points may be identified on the experimental pullout diagrams of inclined steel fibers with hooked ends (Fig. 5).

The initial branch of the pullout response is similar to the one denoted by inclined straight fibers. When fiber debonding occurs (H_1 in Fig. 5) the pullout response enters into an unstable phase in which bending of the debonded segments of the fiber tends to impose failure

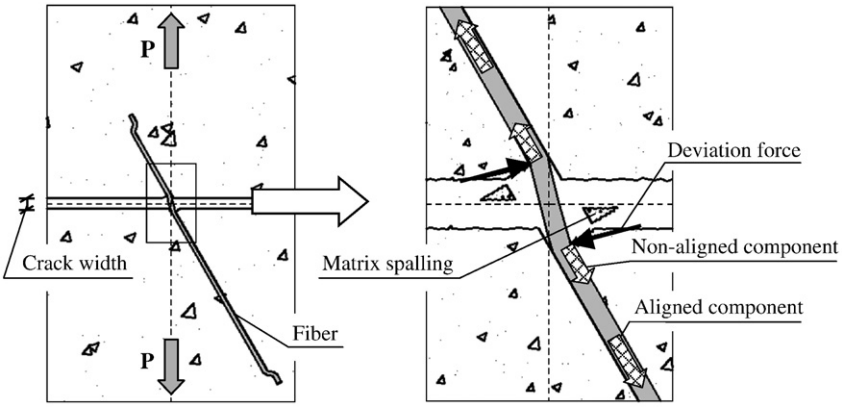

Fig. 4. Pullout of an inclined fiber with matrix spalling at both sides of the cracked surface.

of the matrix at the cracked surface. Depending on the flexibility of the fiber different distribution of pressures and volumes of matrix wedge may be mobilized. Since the respective equivalent force depends upon the fiber axial stress, matrix spalling can then be conceptually divided in two stages: (1) due to axial stress developed along fiber straight segments; (2) due to the increment of axial stress provided by the hook.

Contrarily to straight fibers, at the end of the first stage of matrix spalling (H_2 in Fig. 5) equilibrium at fiber exit point is no longer guaranteed since the hook has already been partially activated. The larger the inclination angle, the larger are the matrix spalling effects and the smaller is the contribution provided by the hook at point H_2.

Matrix spalling moves fiber exit point from the initial pullout axis into sections whose depth respect to cracked surface is progressively higher. Thereby matrix stability increases with the amount of spalling. When the maximum contribution provided by the hook is attained (H_3 in Fig. 5) no further spalling occurs and pullout develops under a more stable mechanism. The post-peak branch is then characterized by three key-points (H_4, H_5 and H_6 in Fig. 5) whose relative slippages are associated to the geometry of the hook.

When the end tip of the fiber enters the initially straight segment of the duct (H_6 in Fig. 5) no further plastic deformations occur. Then friction becomes the dominant mechanism and the load carrying capacity decreases proportionally to the available embedded length at an almost constant rate. When the remaining embedded length tends to zero the pullout load depends mainly on the deviation force at fiber exit point. Thus when a critical embedded length is reached (H_7 in Fig. 5) the load sharply decreases to zero (H_8 in Fig. 5). The latter tends to occur at crack widths of about the initial embedded length deducted by the total length of spalled matrix measured along fiber main axis.

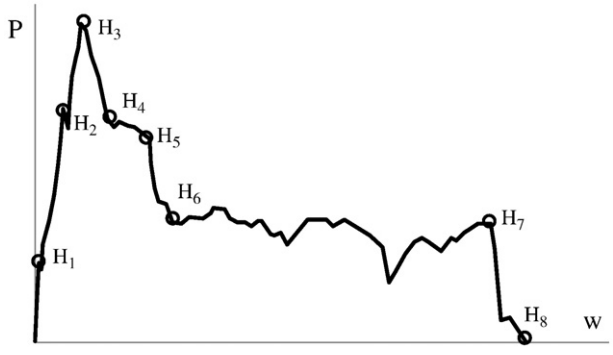

Fig. 5. Identification of the key-points on the experimental pullout response of inclined steel fibers with hooked ends obtained from [5].

4. Pullout model

4.1. General methodology

The pullout response of fibers aligned with the load direction is firstly evaluated and the contribution of the hook along the load-crack width diagram is taken into account through four key-points. Then this contribution is superposed over the pullout response of inclined straight fibers, thus clearly providing the effect of the anchoring mechanism on the pullout diagram. The latter is composed by eight key-points (Fig. 5), each of them related to a different stage of the pullout process. These key-points are then used to trace the predictive pullout responses of inclined fibers.

The focus of the model is on steel fibers with 30–60 mm length and 0.50–1.00 mm diameter embedded in concrete matrices whose compressive strengths remain below 90 MPa.

4.2. Extracting the contribution of the hook from experimental data

An experimental evaluation of the contribution provided by the hook is an absolutely necessary procedure. One of the main reasons for this requirement regards the dissimilar performances exhibited by different types of commercial fibers, which differ both in the quality of the steel and on the geometry of the hook itself. The other major cause is related to the need of testing fibers embedded in representative matrices that reflect the actual characteristics affecting fiber pullout (ex: aggregate grading and maximum grain size, presence of microfibers in the pullout medium, matrix shrinkage, etc.).

In order to evaluate the effect of the hook some authors [3,11] adopted a procedure which consists of subtracting the pullout curve of aligned straight fibers to the respective diagram of fibers with hooked ends. Given that the pullout responses of hooked fibers aligned with the load direction depend mostly on the geometry of the hook, the shape of the pullout responses in these cases are well-known in literature. Thereby, the contribution of the hook is quantified in this model by means of four key-points (Fig. 6).

The initial strengthening provided by the hook is assessed through the increments of pullout load (ΔP_{H01}) and slip at peak (Δw_{H01}) according to Eqs. (1), (2), respectively (Fig. 6).

$$\Delta P_{H01} = P_{H01} - P_{S01} \tag{1}$$

$$\Delta w_{H01} = w_{H01} - w_{S01} \tag{2}$$

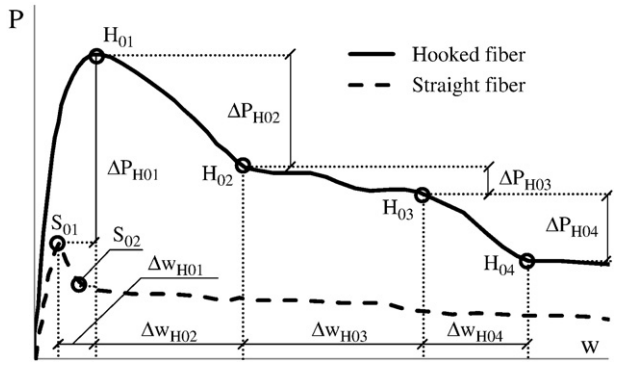

Fig. 6. Identification of the key-points on experimental data of aligned fibers obtained from [11].

The identification of the post-peak key-points (H_{02}, H_{03} and H_{04}) is performed through their relative pullout loads and respective crack widths, such as defined in Eqs. (3), (4) (Fig. 6):

$$\Delta P_{H0(i+1)} = P_{H0(i+1)} - P_{H0i} \tag{3}$$

$$\Delta w_{H0(i+1)} = w_{H0(i+1)} - w_{H0i} \tag{4}$$

With i ranging from 1 to 3. The relative crack widths (Eqs. (2) and (4)) are related to the geometry of the hook and therefore no significant differences respect to values advanced in Fig. 2 should exist.

4.3. Detailed description of the pullout model

Using the experimental data (H_{01}, H_{02}, H_{03} and H_{04} in Fig. 6), the pullout model becomes defined by eight key-points, such as highlighted in Fig. 5. In cases where post-peak accuracy is not fundamental, a simplistic variant of the model can be applied by taking into account uniquely H_{01} and H_{04}. In such case, the pullout model only comprises six key-points (H_4 and H_5 are neglected).

4.3.1. Point H_1: debonding process

The first pullout stage evolves from crack propagation and subsequent fiber activation. Whenever crack passes through the fiber at any of its straight segments (excluding hooked segments) the pullout performance of hooked fibers prior to the beginning of debonding process does not differ from the one of straight fibers.

Hence the first key-point (H_1) is defined just like in the case of straight fibers [14] by Eqs. (5) and (6). This way, factors such as the microstructure of the interfacial transition zone, fiber surface treatments or fiber Poisson's ratio could be covered.

$$P_{H1} = P_{S1} = P_{S01}\cos\theta \tag{5}$$

$$w_{H1} = w_{S1} = w_{S01} \tag{6}$$

4.3.2. Point H_2: effects of matrix spalling (stage 1)

In the model advanced for straight steel fibers [14], the length of spalled matrix (L_{SP1}) was calculated through a failure criterion which considered, on one side, the tensile strength and the geometric configuration of the matrix wedge at the cracked surface and, on the other side, a spalling force (F_{SP1}) dependent on the deviation force at fiber exit point. A similar phenomenon is observed in the pullout of hooked fibers. Matrix spalling extends under increasing pullout loads such that when the contribution along the fiber main axis equalizes the one observed in straight fibers (P_{S01}) the length of the spalled matrix might be suchlike (L_{SP1}). However, at the end of the first stage of matrix spalling process (point H_2) the anchorage effect provided by the hook might have introduced some resistance against fiber slippage. Accordingly, it will be assumed that the hook is activated just after fiber debonding (point H_1) and its contribution increases progressively until a maximum value along fiber main axis (P_{H01}) is observed (point H_3).

In the case of fibers under large inclination angles, local friction at the fiber exit point governs the pullout process, thus postponing the anchoring effect provided by the hook. According to the model advanced for straight fibers [14] the balance between the aligned and non-aligned components of the pullout mechanism at the end of the first stage of matrix spalling is proportional to the spalling length (L_{SP1}). Thereby the aligned component of the pullout load (P_{HA2}) becomes defined as following:

$$P_{HA2} = \left(P_{S01}L_{eff(H2)} + \Delta P_{H01}\frac{L_e - 6\times L_{SP1}}{L_e}\right)\cos\theta \tag{7}$$

Where $L_{eff\,(H2)}$ is the effective length factor taking into account the reduction of available embedded length (Eq. (8)):

$$L_{eff(H2)} = L_{eff(S2)} = \left(\frac{L_e - L_{SP1}}{L_e}\right) \tag{8}$$

P_{S01} applies for the straight segment of the fiber since sliding is restrained by the hook. The non-aligned component of the pullout (P_{HN2}) accounts uniquely for the deviation force (D_{F1}) which equilibrates the respective spalling force (F_{SP1}), such as defined in Eq. (9):

$$P_{HN2} = P_{SN} = \mu D_{F1} = \mu P_{S01}\sin\theta\cos\frac{\theta}{2} \tag{9}$$

The pullout load at this stage is then obtained by summing Eqs. (7) and (9):

$$P_{H2} = P_{HA2} + P_{HN2} \tag{10}$$

The respective crack width (w_{H2}) is defined consistently by considering the contribution derived from the aligned component (w_{HA2}) and the increment due to matrix spalling (Δw_{SP1}):

$$w_{H2} = w_{HA2} + \Delta w_{SP1} \tag{11}$$

The portion of the crack width which accounts for the effects occurring along the embedded fiber axis (w_{HA2}) includes the crack width associated to the debonding process (w_{H1}) and the increment of crack width due to partial deformation of the hook (Eq. (12)).

$$w_{HA2} = w_{H1} + \Delta w_{H01}\frac{L_e - 6\times L_{SP1}}{L_e}\cos\theta \tag{12}$$

The increment of crack width accounting for the reorientation of the fiber due to the first stage of matrix spalling (Δw_{SP1}) is the one defined for straight fibers:

$$\Delta w_{SP1} = N L_{SP1}(1-\cos\theta) \tag{13}$$

Where N is the number of sides of the crack where spalling occurs ($N=1$ or $N=2$).

4.3.3. Point H_3: effects of matrix spalling (stage 2)

The anchoring effect provided by the hooks increases significantly stresses on the fiber and consequently matrix undergoes a second stage of spalling until the maximum force along fiber main axis (P_{H01}) is equilibrated at the new fiber exit point. To account for the increment of spalled matrix along fiber main axis (L_{SP2}) a simplified failure criterion was adopted (Appendix 2). The pullout load at the

end of the second stage of matrix spalling (P_{H3}) is then obtained by summing the respective aligned (P_{HA3}) and non-aligned (P_{HN}) components. The former takes into account the increment of strength provided by the hook such as measured on experimental data (ΔP_{H01}) as well as the contribution provided by the straight segments of the fiber, affected by the reduction of embedded length due to matrix spalling:

$$P_{HA3} = \left(P_{S01} L_{eff(H3)} + \Delta P_{H01}\right)\cos\theta \tag{14}$$

Where $L_{eff\ (H3)}$ is the effective length factor at key-point H_3, defined as following:

$$L_{eff(H3)} = \frac{L_e - (L_{SP1} + L_{SP2})}{L_e} \tag{15}$$

Although full-debonding has already occurred at this stage, P_{S01} still applies in Eq. (14) since frictional sliding is still restrained due to the presence of the hook.

The non-aligned component of the pullout mechanism (P_{HN}) stands for the local friction introduced by the new deviation force (D_{F2}) which depends upon the maximum axial force on the fiber (P_{H01}) and on the deviation angle between the embedded and protruded lengths of the fiber (Eqs. (16), (17)).

$$P_{HN} = \mu D_{F2} \tag{16}$$

$$D_{F2} = P_{H01}\sin\theta\cos\frac{\theta}{2} \tag{17}$$

The crack width at which the peak pullout load occurs (w_{H3}) accounts for the crack width prior to debonding (w_{H1}) and for its increment due to straightening of the hook, such as measured in the experimental data (Δw_{H01}). Furthermore it also considers the increments of crack width due to both stages of matrix spalling, being the latter defined in Eq. (18). Hence w_{H3} becomes the sum of the multiple components, such as shown in Eq. (19).

$$\Delta w_{SP2} = N L_{SP2}(1-\cos\theta) \tag{18}$$

$$w_{H3} = w_{H1} + \Delta w_{H01}\cos\theta + \Delta w_{SP1} + \Delta w_{SP2} \tag{19}$$

4.3.4. Point H_4: post-peak (stage 1)

Once the maximum contribution provided by the hook is attained (point H_3) the decrease on the pullout load is similar to the one observed on the post-peak branch of aligned fibers (Fig. 6). In the absence of further matrix spalling the curvature of fiber at the exit point remains unchanged and therefore a constant non-aligned component will be assumed (P_{HN}). On the other hand, the aligned contribution (P_{HA4}) becomes defined such as shown in Eq. (20):

$$P_{HA4} = \left(P_{S01} L_{eff(H4)} + \sum_{i=1}^{2} \Delta P_{H0i}\right)\cos\theta \tag{20}$$

Where $L_{eff\ (H4)}$ is the effective length factor at key-point H_4:

$$L_{eff(H4)} = \frac{L_e - (L_{SP1} + L_{SP2} + \Delta w_{H02})}{L_e} \tag{21}$$

Regarding that after peak load no further matrix spalling occurs, the crack width at this stage (w_{H4}) is obtained by adding to the previous stage the increment derived from the straightening of the hook, such as defined in Eq. (22).

$$w_{H4} = w_{H3} + \Delta w_{H02}\cos\theta \tag{22}$$

4.3.5. Point H_5: post-peak (stage 2)

The second stage of the post-peak branch is defined on a comparative way relatively to point H_4. The pullout load accounts for the deviation force at fiber exit point (P_{HN}) and for a reduced aligned contribution (P_{HA5}):

$$P_{HA5} = \left(P_{S01} L_{eff(H5)} + \sum_{i=1}^{3} \Delta P_{H0i}\right)\cos\theta \tag{23}$$

Where $L_{eff\ (H5)}$ is the effective length factor at key-point H_5:

$$L_{eff(H5)} = \frac{L_e - \left(L_{SP1} + L_{SP2} + \sum_{i=2}^{3} \Delta w_{H0i}\right)}{L_e} \tag{24}$$

The crack width at which the second post-peak stage occurs (w_{H5}) is obtained by summing the respective slippage of the hook in that phase (Eq. (25)).

$$w_{H5} = w_{H4} + \Delta w_{H03}\cos\theta \tag{25}$$

4.3.6. Point H_6: post-peak (stage 3)

Analogously to previous post-peak stages, the load at point H_6 also accounts for the non-aligned component (P_{HN}) and for an aligned contribution (P_{HA6}):

$$P_{HA6} = \left(P_{S02} L_{eff(H6)} + \sum_{i=1}^{4} \Delta P_{H0i}\right)\cos\theta \tag{26}$$

Where $L_{eff\ (H6)}$ is the effective length factor at key-point H_6:

$$L_{eff(H6)} = \frac{L_e - \left(L_{SP1} + L_{SP2} + \sum_{i=2}^{4} \Delta w_{H0i}\right)}{L_e} \tag{27}$$

The interface properties at the straight segments of the fiber are now represented by P_{S02} assuming that the fiber is subjected uniquely to frictional sliding. The load at this stage comprises the contribution provided by the deviation force at the fiber exit point, the residual friction provided by incomplete straightening of the hook and also friction along the straight segments of the fiber. The respective crack width is obtained as following:

$$w_{H6} = w_{H5} + \Delta w_{H04}\cos\theta \tag{28}$$

4.3.7. Point H_7: pre-removal stage

At the end of the pullout process the hook portion becomes progressively closer to the cracked surface. The pullout load (P_{H7}) is then provided both by the component derived from the deviation force (P_{HN}) and by the aligned component (P_{HA7}), which depends majorly on the residual contribution of the hook (Eq. (29)).

$$P_{HA7} = \left(\sum_{i=1}^{4} \Delta P_{H0i}\right)\cos\theta \tag{29}$$

When the hook starts being removed, the three-point mechanism turns into two single points of contact (G_1 and G_2 in Fig. 3). Whenever the remaining embedded length equalizes the distance between these two points ($L_{H,crit}$) an unstable mechanism is generated. Fiber end tip tends then to rotate and the friction generated may increase locally

the pullout load. The crack width at which this process of fiber removal begins (w_{H7}) is defined by Eq. (30).

$$w_{H7} = L_e - \left(L_{SP1} + L_{SP2} + L_{H,crit}\right) \quad (30)$$

Where $L_{H,crit}$ is the distance between sections G_1 and G_2 (approx. 2.0 mm in Fig. 1).

4.3.8. Point H_8: removal from the matrix

Upon the beginning of the fiber removal process, the pullout load drops sharply to a zero value within a crack width range of about the critical length ($L_{H,crit}$). Consequently, P_{H8} and w_{H8} become defined by:

$$P_{H8} = 0 \quad (31)$$

$$w_{H8} = L_e - (L_{SP1} + L_{SP2}) \quad (32)$$

4.4. Parameter identification

This model is based on the following input parameters:

- Fiber diameter (d), embedded length (L_e) and tensile strength (σ_u).
- Average tensile strength of the cement matrix (f_{ctm})
- Experimental key-points from the pullout of aligned fibers (straight and hooked geometries).

The proposed pullout diagram for inclined fibers is shown in Fig. 7, whose shape is governed by the eight highlighted key-points, summarized in Table 1 for convenience. The several stages of the pullout process represented by each key-point are depicted in Fig. 8 in order to provide a better understanding on the physical mechanisms involved.

To generalize the model to any hooked fiber embedded in a cement matrix, the model has to include scenarios in which insufficient fiber embedded length induces earlier removal of the fiber and the case of rupture of a fiber due to attainment of its rupture load at a certain inclination angle ($P_u(\theta)$). Furthermore, the shape of the pullout response at the pre-peak branch may vary depending on whether it is governed by matrix spalling effects or by the straightening of the fiber hook. These three cases are considered in the model through the conditions described in the following.

4.4.1. Fiber rupture condition

Contrarily to straight steel fibers, in which fiber tensile strength does not play a major role, the significant anchorage effect provided by the hooked ends converts $P_u(\theta)$ into a paramount parameter to evaluate the pullout of inclined steel fibers. Regarding the intricacy of the phenomenon a simplified heuristic procedure was adopted to quantify the inclined tensile strength at any inclination angle, $\sigma_u(\theta)$, as shown in Appendix 3. Thereby the key-points described in Table 1 apply whenever the maximum pullout load at a certain inclination angle is lower than the correspondent ultimate pullout load:

$$P_{H3} < P_u(\theta) \quad (33)$$

In cases where Eq. (33) is not verified the pullout model accounts uniquely for points H_1, H_2 and the point at which fiber fails, defined by $P_u(\theta)$ and a respective crack width obtained by linear interpolation (Eq. (34)):

$$w_u(\theta) = w_{H2} + \frac{P_u(\theta) - P_{H2}}{P_{H3} - P_{H2}}(w_{H3} - w_{H2}) \quad (34)$$

4.4.2. Available embedded length condition

In order to provide a better understanding on the influence of each phenomenon in the pullout response, the formulation of the model key-points was performed in an additive form. Likewise, the extent of the post-peak range depends upon the available fiber embedded length after the occurrence of matrix spalling. In cases where the initial fiber embedded length is small and/or the matrix spalling lengths are significant, the post-peak range may be severely reduced or completely vanished. The latter may also compromise the complete mobilization of the hooked end and therefore the maximum pullout load has to be reduced accordingly. Hence model predictions are based on the key-points defined in Table 1 whenever the Eq. (35) is verified for all j between 1 and 6.

$$w_{H7} > w_{Hj} \quad (35)$$

In case that one or more points do not obey Eq. (35) it means that earlier removal of the fiber occurs and that the hooked end is not fully mobilized. In such conditions a new and simplified pullout diagram applies taking into account only the points which verify Eq. (35) and the ones corresponding to the stage of fiber removal (H_7 and H_8),

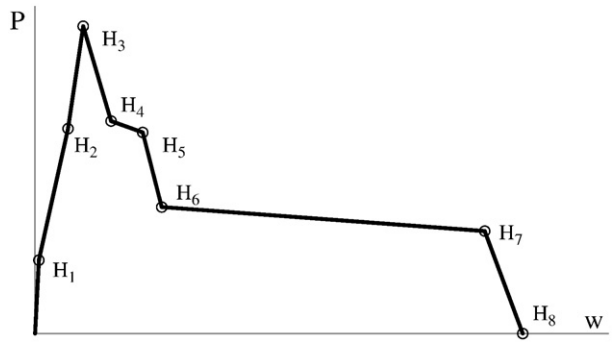

Fig. 7. Schematic diagram of the pullout model for inclined fibers with hooked ends.

Table 1
Summary of expressions which define the pullout model.

Point	Formulation
H_1	$P_{H1} = P_{S01}\cos\theta$ $w_{H1} = w_{S01}$
H_2	$P_{H2} = \left(P_{S01}L_{eff(H2)} + \Delta P_{H01}\frac{L_e - 6\times L_{SP1}}{L_e}\right)\cos\theta + \mu D_{F1}$ $w_{H2} = w_{H1} + \Delta w_{H01}\cos\theta\frac{L_e - 6\times L_{SP1}}{L_e} + \Delta w_{SP1}$
H_3	$P_{H3} = (P_{S01}L_{eff(H3)} + \Delta P_{H01})\cos\theta + \mu D_{F2}$ $w_{H3} = w_{H1} + \Delta w_{H01}\cos\theta + \Delta w_{SP1} + \Delta w_{SP2}$
H_4	$P_{H4} = \left(PS01L_{eff(H4)} + \sum_{i=1}^{2}\Delta P_{H0i}\right)\cos\theta + \mu D_{F2}$ $w_{H4} = w_{H3} + \Delta w_{H02}\cos\theta$
H_5	$P_{H5} = \left(P_{S01}L_{eff(H5)} + \sum_{i=1}^{3}\Delta P_{H0i}\right)\cos\theta + \mu D_{F2}$ $w_{H5} = w_{H4} + \Delta w_{H03}\cos\theta$
H_6	$P_{H6} = \left(P_{S02}L_{eff(H6)} + \sum_{i=1}^{4}\Delta P_{H0i}\right)\cos\theta + \mu D_{F2}$ $w_{H6} = w_{H5} + \Delta w_{H04}\cos\theta$
H_7	$P_{H7} = \left(\sum_{i=1}^{4}\Delta P_{H0i}\right)\cos\theta + \mu D_{F2}$ $w_{H7} = L_e - (L_{SP1} + L_{SP2} + L_{H,crit})$
H_8	$P_{H8} = 0$ $w_{H8} = L_e - (L_{SP1} + L_{SP2})$

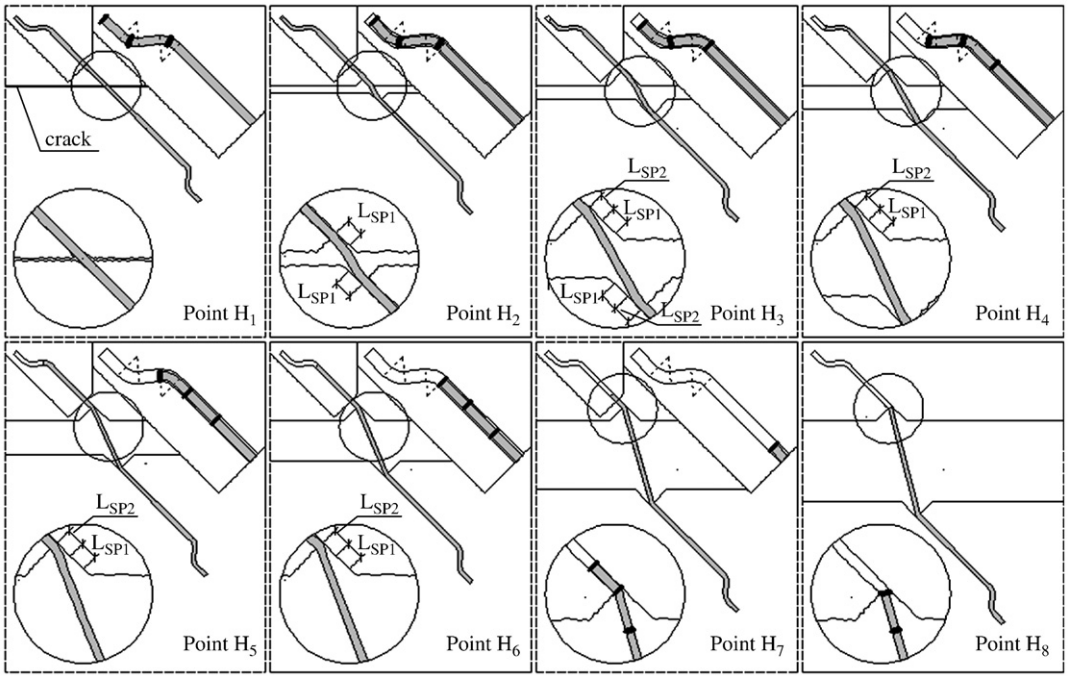

Fig. 8. Main stages of the pullout process of inclined fibers and associated model key-points.

starting at crack width w_{H7} and with a respective pullout load such as defined in Eq. (36):

$$P_{H7} = P_{Hj} + \left(P_{H(j+1)} - P_{Hj}\right)\frac{w_{H7} - w_{Hj}}{w_{H(j+1)} - w_{Hj}} \tag{36}$$

Where j corresponds to the higher numbered key-point at which Eq. (35) is verified.

4.4.3. Shape of the pullout response

Once the thorough set of key-points is defined, the pullout response of inclined steel fibers can be approximated by a multi-linear diagram such as shown in Fig. 7. Although this is a quite straightforward procedure, one should be aware of the approximations that are being introduced, particularly within the range of crack widths with interest for structural applications.

When observing the pullout of aligned fibers (Fig. 6) it can be observed a non-linear pre-peak behavior due to the straightening of the hook. Consequently, on fibers under small inclination angles (whose pullout mechanisms are governed by the aligned component), a multi-linear assumption would underestimate the load carrying capacity of those fibers. To overcome this limitation, the pullout diagram in the pre-peak branch (from H_1 to H_3 in Fig. 7) may be defined depending on the dominance either of the spalling mechanisms or, alternatively, of the hook's deformation on the crack width at peak. Thereby, the interpolation between key-points H_1 to H_3 should respect the following condition:

$$\begin{cases} \Delta w_{SP1} + \Delta w_{SP2} \geq \Delta w_{H01} \Rightarrow \text{Bi} - \text{linear branch} \\ \Delta w_{SP1} + \Delta w_{SP2} < \Delta w_{H01} \Rightarrow \text{Parabolic branch} \end{cases} \tag{37}$$

When the spalling effects are relatively reduced the parabolic expression may be obtained by means of the coordinates at points H_1 and H_3 and by fixing the derivate at peak (H_3) equal to zero. Note that, in this case, the use of a non-linear pre-peak branch disregards the calculation of H_2.

5. Model validation

In order to ascertain the suitability of the proposed approach on describing the pullout response of inclined fibers, different experimental results from literature are taken into account [4,5]. The experimental data herein presented considers hooked fibers with different diameters, tensile strengths and embedded lengths within different cement matrices.

5.1. Robins et al. [4]

The experimental research carried out by these authors evaluates the influence of fiber inclination angle, fiber embedded length and type of matrix on the load-crack with response. In their work specimens were cast in two stages, firstly with the matrix for testing and then using a high strength mortar to guarantee that pulling out of the fiber occurred uniquely from one side of the specimen. A brass with a 10 mm hole in the center was inserted to provide continuity and to form a reduced section at which matrix cracked. Fibers with 50 mm length were inserted within the matrix at 5, 10, 15 and 20 mm embedded lengths under inclination angles of 0°, 10°, 20°, 30°, 40°, 50° and 60°. The average results considered hereafter are the outcome of four specimens with concretes of 72 MPa average compressive strength. The procedure described in Section 4.2 was applied to extract the experimental input values from the pullout of aligned fibers ($\theta = 0°$). A summary of the values used on this model validation is presented in Appendix 4.

The initiation of debonding occurs whenever crack is deflected along the fiber–matrix interface, which corresponds to the minimum post-peak value of the load-crack width response [19]. According to experimental results the crack width at that minimum was between 0.020 and 0.050 mm and the respective load between 10 and 40 N. w_{S01} and P_{S01} will then be roughly approximated as 0.035 mm and 25 N, respectively. In the absence of experimental values for straight fibers, the crack width at the beginning of friction stage (w_{S02}) will be assumed as 0.3 mm and the respective load (P_{S02}) as half of the peak value (P_{S01}). Comparisons between model predictions and experimental results are shown in Figs. 9–12, in which good agreement of the pullout diagrams can be seen in most of the cases.

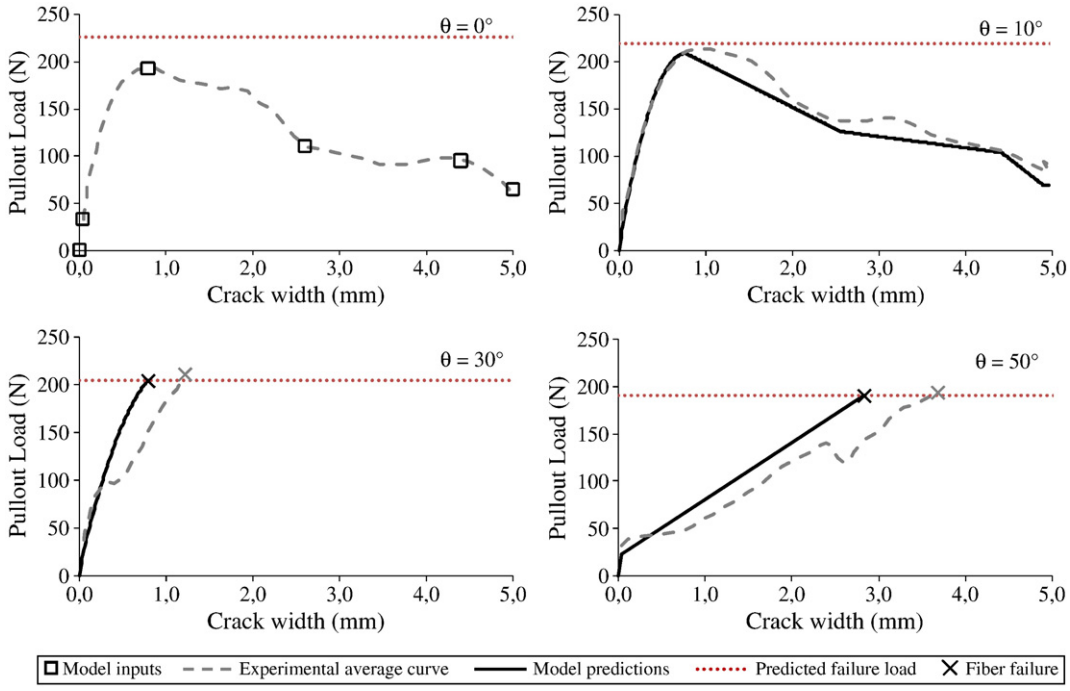

Fig. 9. Model validation over experimental results from [4] for 20 mm fiber embedded length.

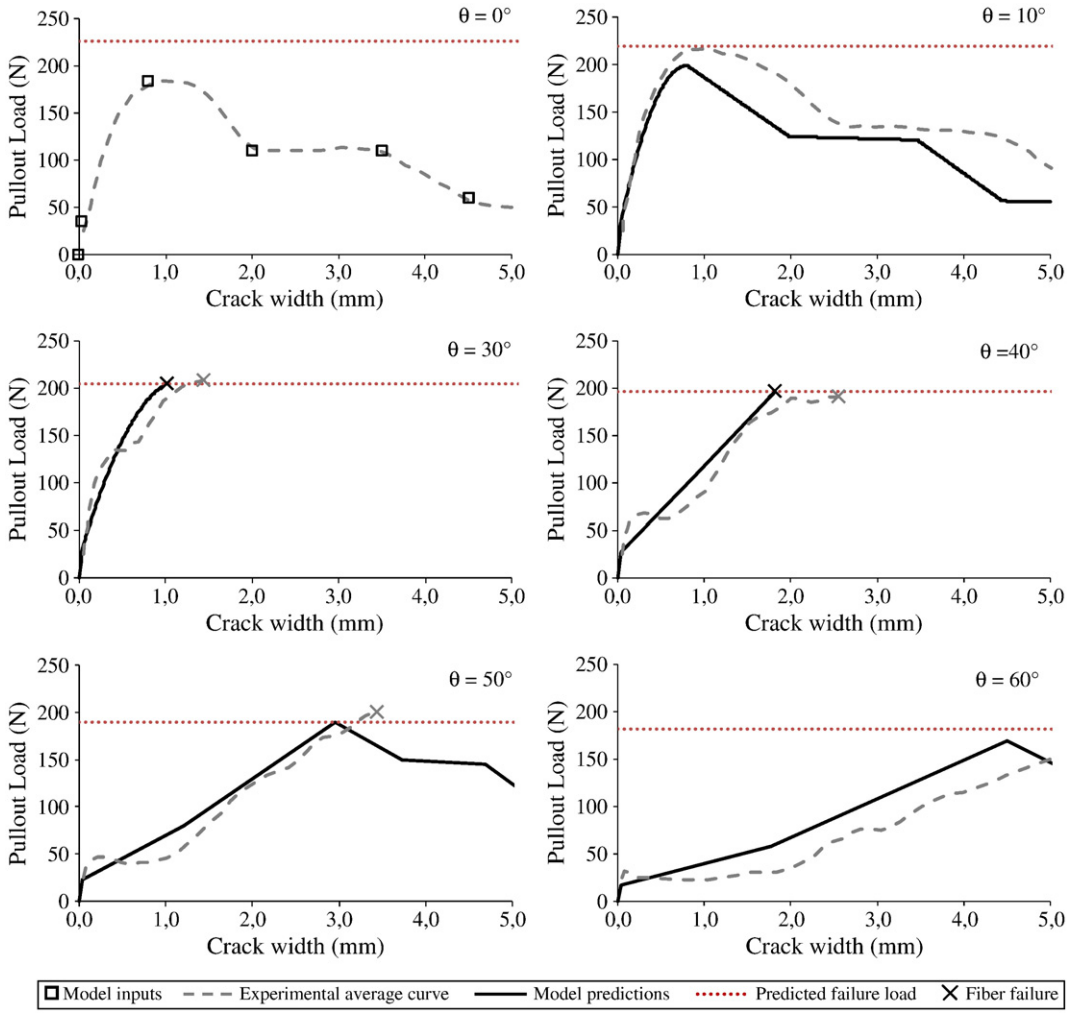

Fig. 10. Model validation over experimental results from [4] for 15 mm fiber embedded length.

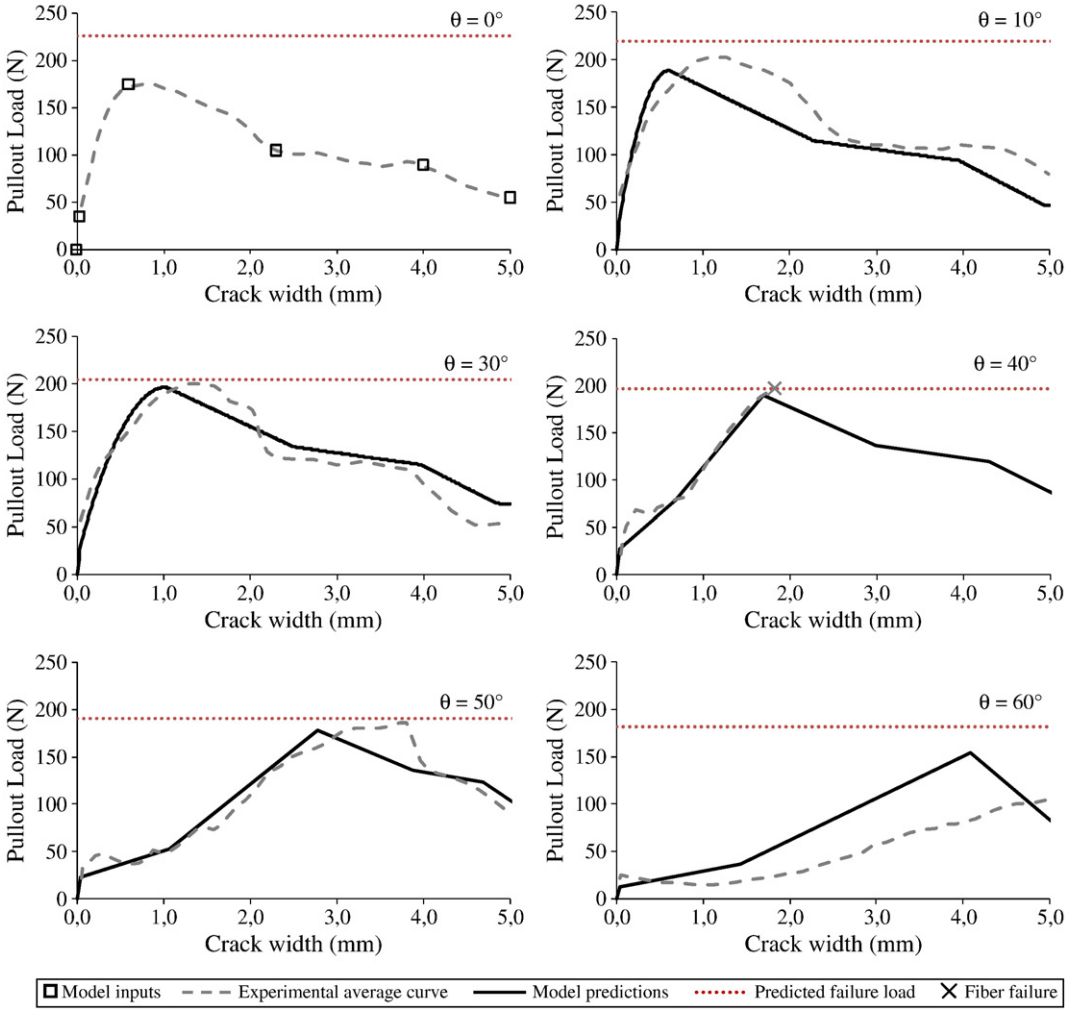

Fig. 11. Model validation over experimental results from [4] for 10 mm fiber embedded length.

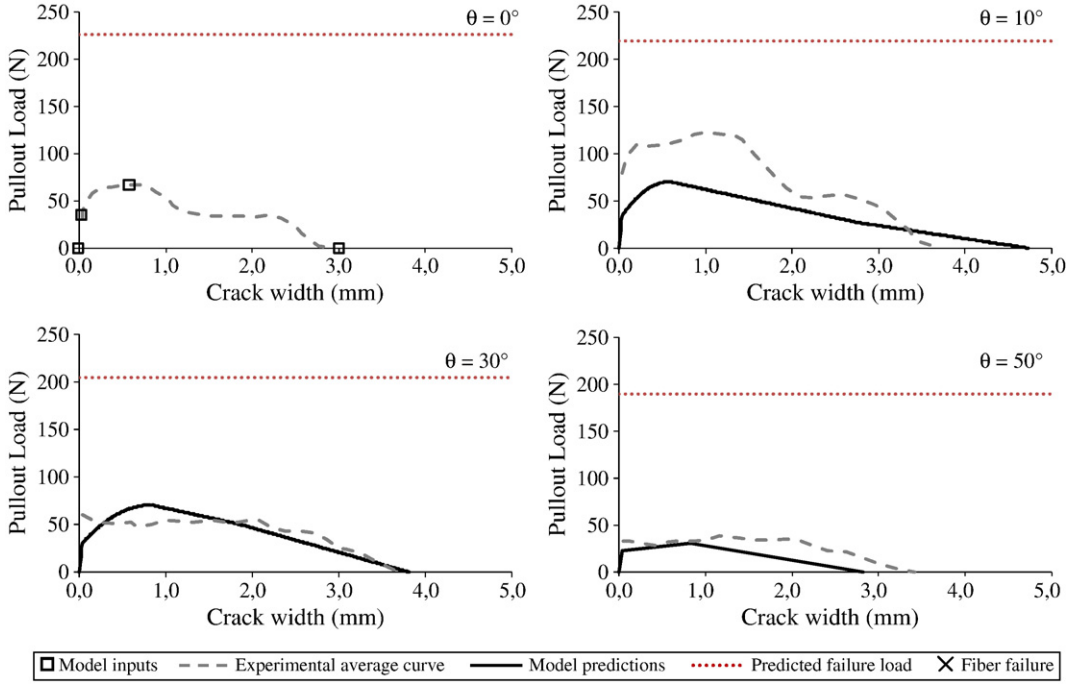

Fig. 12. Model validation over experimental results from [4] for 5 mm fiber embedded length.

The pullout model is able to reproduce the postponed activation of the mechanical anchorage at increasing inclination angles (Figs. 9–11). Predicted crack widths at peak increased more than proportionally with the inclination angle as a result of the magnification of matrix spalling. In cases of fibers at 10° and 30° the spalled lengths of the matrices are not significant and, consequently, the predictions provided by the model consider a non-linear pre-peak branch, such as previously suggested in Eq. (37). With this criterion, the model approximates with good accuracy the pre-peak branch of all fibers, irrespectively of the governing pullout mechanisms.

At larger crackwidths, the post-peak range up to complete straightening of the hook is reasonably well predicted for fibers with small inclination angles, at least for the available crack width range of comparison (5 mm).

According to experimental values, fibers with embedded lengths greater than 5 mm and inclination angles larger than 20° were likely to have their peak loads limited by fiber rupture. Such trend is also successfully reproduced, although in some cases a slight overestimation of fiber's rupture load leads to post-peak branches on the pullout model.

The pullout response of fibers under large inclination angles seems to be significantly overestimated by the model. However it should be pointed out that the scattering of experimental results was reported to increase significantly with fiber inclination angles, reaching coefficients of variation for the pullout response between 25 and 50% for fibers at 60° inclination angle.

To evaluate the suitability of the model in describing the main features of the pullout response, correlations between the model predictions and average experimental results for peak values and pullout work are shown in Fig. 13. It is evident that pullout responses of fibers at different inclination angles were essentially the same whenever the hook was fully mobilized (Figs. 9–11). On

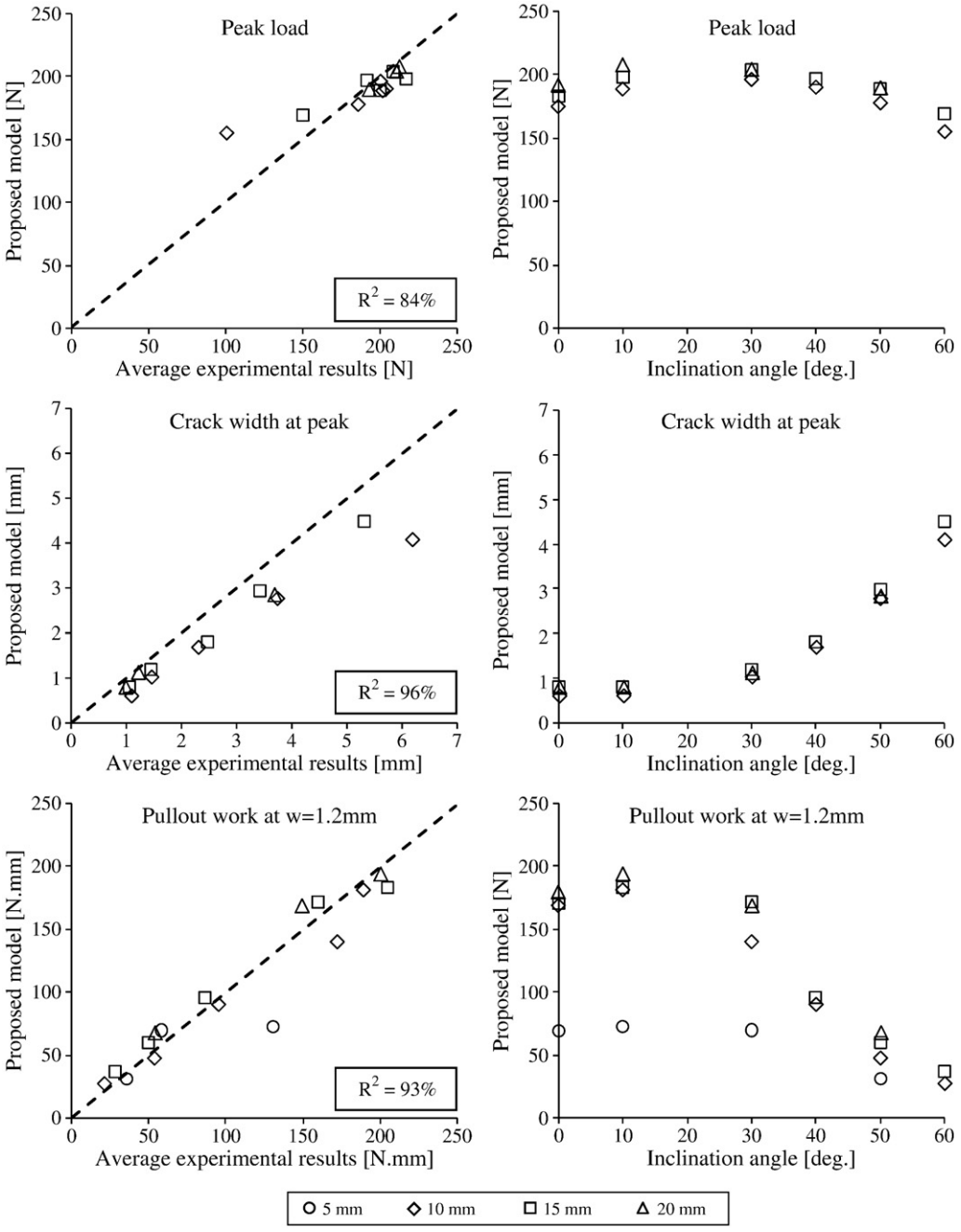

Fig. 13. Comparison between model predictions and experimental results obtained from [4] (left) and influence of fiber inclination angle on the pullout model (right).

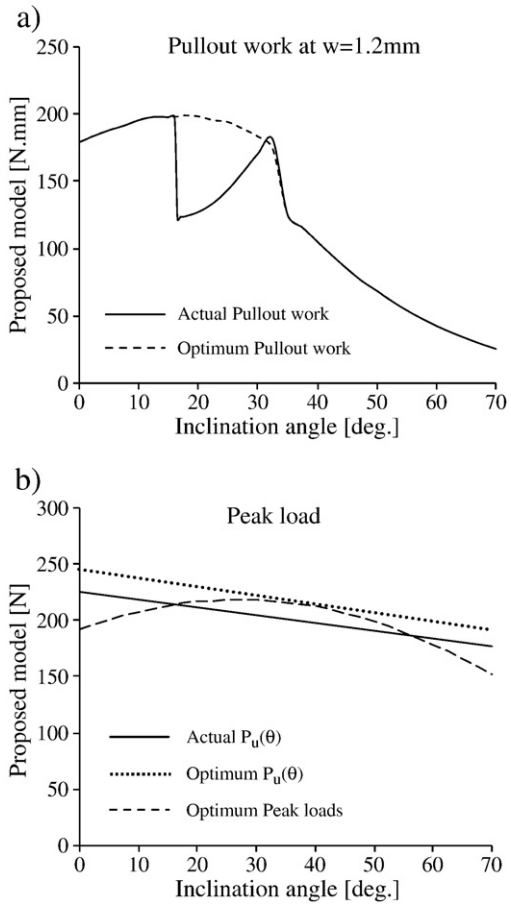

Fig. 14. Study on the influence of fiber tensile strength on peak load and pullout work at different θ.

the other hand, with fibers with 5 mm embedded length (Fig. 12) the mechanical anchorage was not fully developed and therefore pullout performance was rather poor. Moreover uncertainties regarding accurate measurements of the actual embedded length (which in the case of aligned fibers led to complete fiber removal at only 3.0 mm) might also support the significant coefficients of variations observed for this case (10 to 60%). Therefore it is not surprising the lower agreement provided by the model, which even though, is able to reasonably approximate the pullout work in such unsteady conditions (Figs. 12 and 13).

Once analyzing Fig. 13 one should be aware that the experimental failure mode of fibers with inclination angles larger than 20° and embedded lengths greater than 5 mm was mostly by fiber rupture. Given that this is an undesirable failure mode, the pullout model can then be used to provide some valuable insights and optimize the design of SFRC.

According to model predictions, the critical inclination angle (θ_{crit}) above which fiber rupture occurs for fibers with 20 mm embedded length is 16°. Thereby a steep decrease on the pullout work is expected for fibers at larger inclination angles. Such becomes evident in Fig. 14a, where significantly lower pullout works are predicted for angles ranging between 16° and 35°. For angles larger than 35° the pullout work is no longer affected by fiber rupture regarding that the range of crack widths at which it takes place is larger than 1.2 mm.

By performing a simple parametric study it is possible to conclude that, if fiber rupture could be avoided, pullout work at 1.2 mm crack width would be maximized at 17° (199.0 N.mm) and it would be at least as higher than that of aligned fibers (179.3 N.mm) up to 31° (Fig. 14a). With regard to the peak loads (Fig. 14b), they remain larger than those of aligned fibers up to 55° and their optimum range occurs between 25° and 30°, with values about 14% higher than those of aligned fibers.

The maximum difference between peak and fiber rupture loads provides a first step to optimize the tensile strength of steel fibers. In this particular case, the range between 35° and 40° is the one providing minimum safety against fiber rupture. At this angle the peak load would exceed the respective ultimate failure load about 9% (Fig. 14b). Therefore fiber tensile strength would have to be at least 1250 MPa (9% higher) to avoid fiber rupture at any inclination angle.

5.2. Van Gysel [5]

This investigation comprised an extensive experimental work in which fibers with different geometries and tensile strengths were pulled out from two types of mortar matrices. Two diameters of fibers (0.50 and 0.80 mm) were tested at five different angles (0°, 15°, 30°, 45° and 60°) with 30 mm fiber embedded length. Fiber ultimate tensile strengths were 2148 and 2117 MPa for diameters 0.50 and 0.80 mm, respectively. The mean compressive strength of the matrix was about 76.5 MPa and four specimens were tested for each set of parameters. The input values for the pullout model are summarized in Appendix 4.

The pullout responses of aligned fibers were available both for straight and hooked fibers. In the former the peak values reported were considered whereas the friction stage was assumed to start at a crack width of 0.3 mm with 50% of the peak load. With regard to the experimental data of hooked fibers, the procedure described in

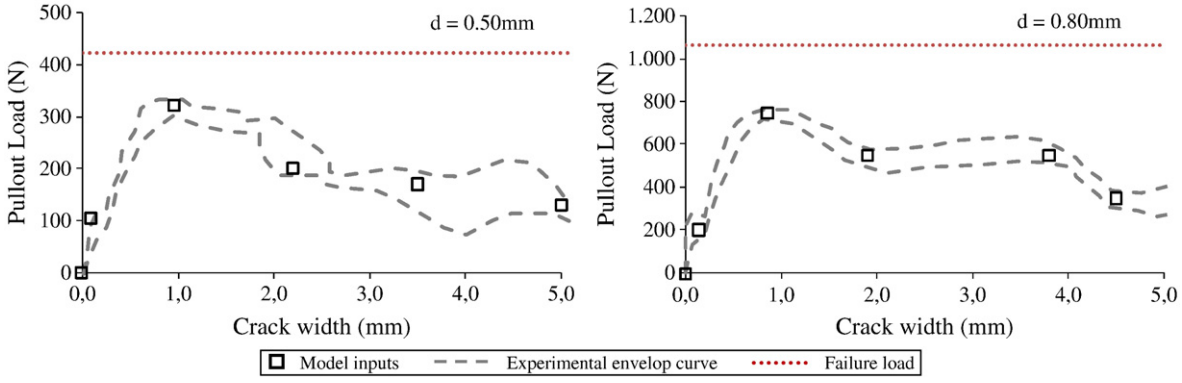

Fig. 15. Extraction of the hook contribution from experimental data on aligned fibers from [5].

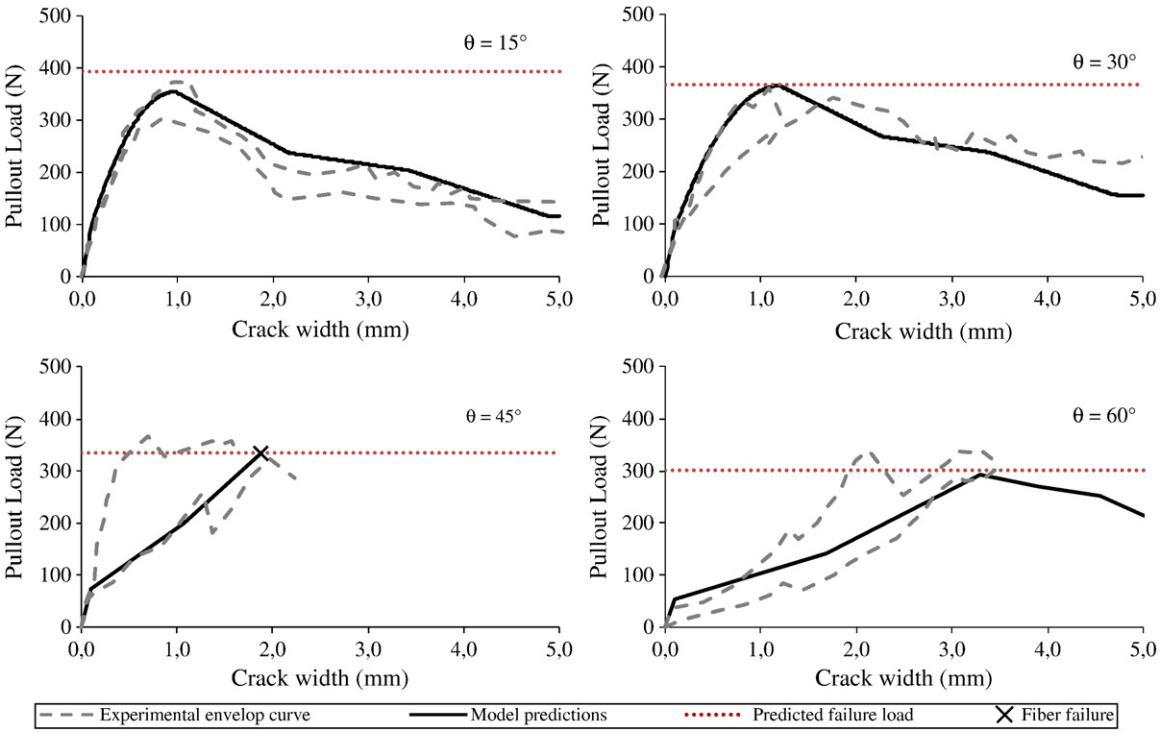

Fig. 16. Model validation over experimental results from [5] for fibers with 0.50 mm diameter.

Section 4.2 was applied to identify the contribution of the hook (Fig. 15).

Pullout responses of fibers with 0.50 mm diameter at different angles are shown in Fig. 16. It can be seen that model predictions fit the range of experimental results along the entire pullout diagram in most cases.

Experimental results at 30° presented a mixed type of rupture, with three fibers failing and one undergoing subsequent pullout. For

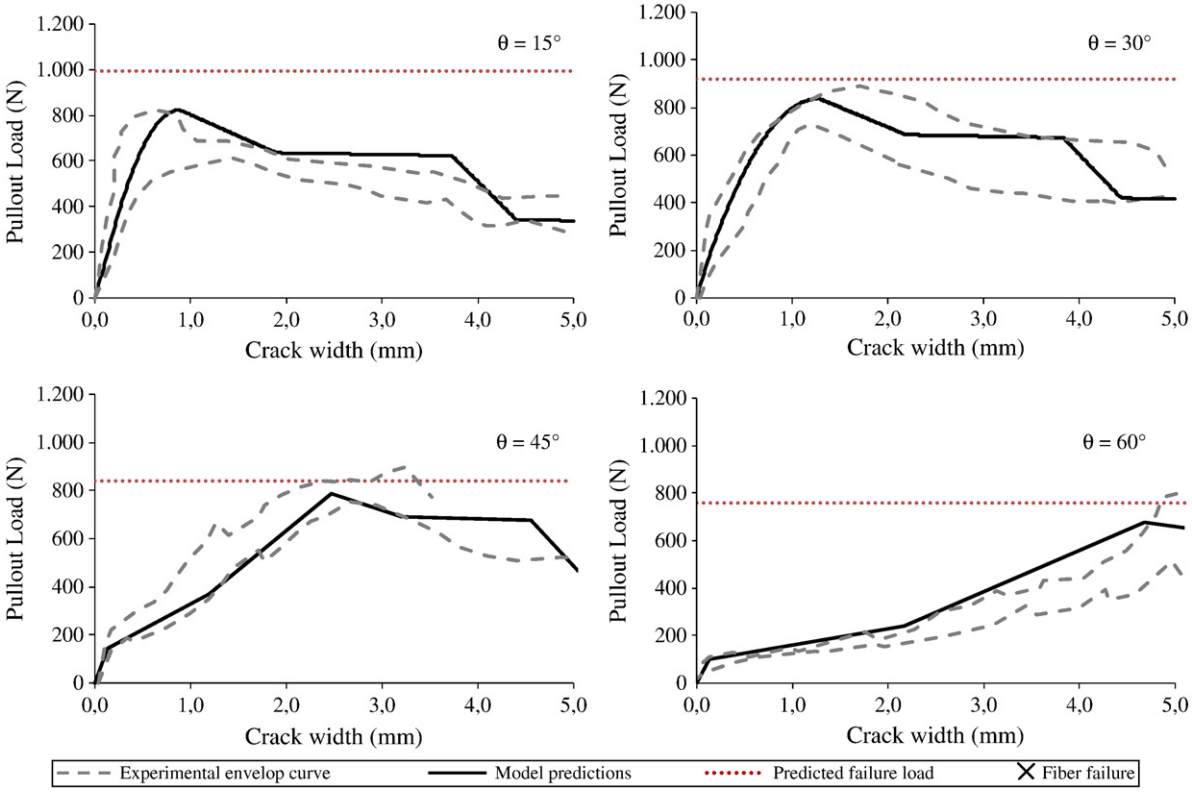

Fig. 17. Model validation over experimental results from [5] for fibers with 0.80 mm diameter.

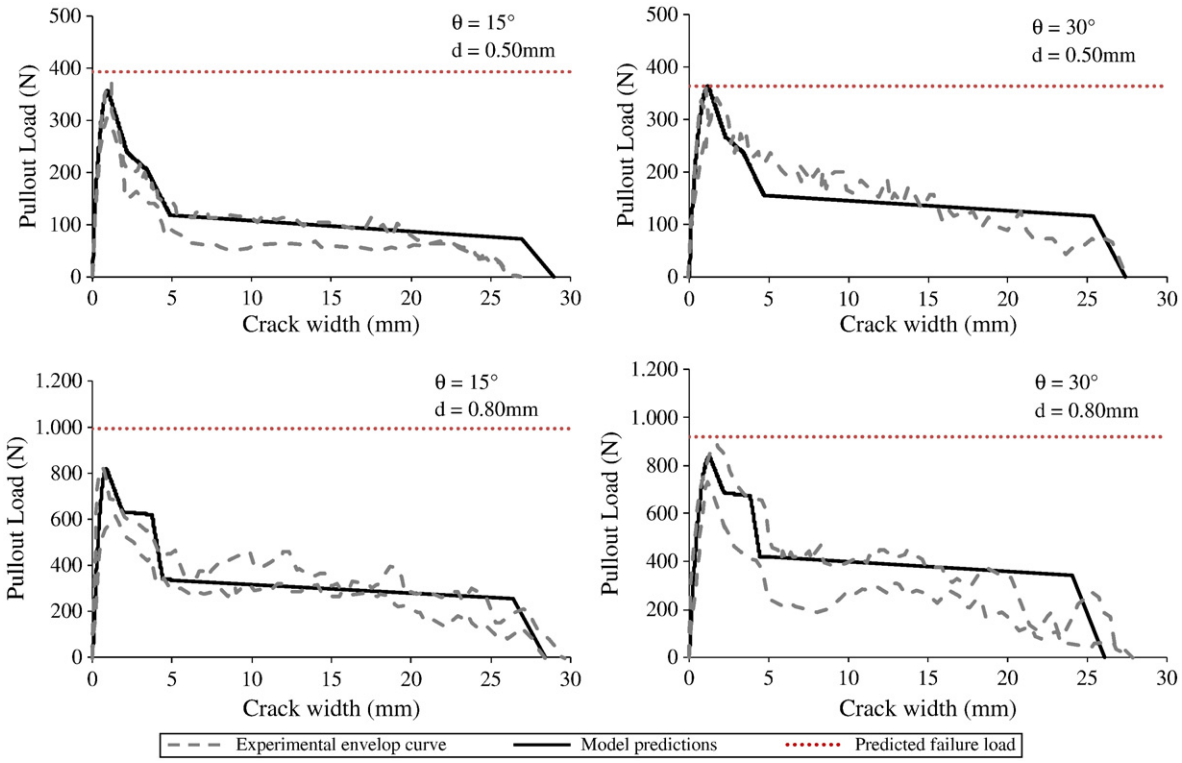

Fig. 18. Model validation over experimental results from [5] up to complete removal of the fiber from the matrix.

this case the pullout model predicted a peak value of about 99% the ultimate load of inclined fibers, thus also denoting an eminent change in the pullout failure mode. Tests on fibers at 45° and 60° present larger scattering along the load-crack width responses and fiber rupture in all situations. Fiber rupture is well predicted for 45° whereas its prominence is evident with fibers at 60°, where the peak load attains about 98% its inclined ultimate load.

Model predictions for fibers with 0.80 mm diameter are also in good agreement with the experimental results (Fig. 17). For fibers with 15° and 30° the experimental post-peak behavior is smoother than predicted by the model. This supports that the simplified version of the model (excluding points H_4 and H_5) would apply in this case with particular good results.

Figs. 16 and 17 show that tests on fibers with 15° and 30° report failure modes in which all fibers, or significant part of them, are pulled out. At least two valid experimental pullout results were reported in this situation, with the exception being fibers with 0.50 mm diameter and 30° which only provided one diagram. In these cases it is possible to validate the model along the entire load-crack width response (Fig. 18). It can be observed in Fig. 18 that a good agreement on the predicted responses also occurs at very large crack widths, with similar performances both on magnitude and slope of the friction branch.

6. Conclusions

In this work a new conceptual approach was advanced to predict the pullout response of inclined steel fibers with hooked ends. The model is based on the most representative geometric and strength properties of the constituent materials and on experimental data of fibers aligned with the load direction. From the latter the contributions provided both by hooked ends and straight segments of the fiber are evaluated. Then fiber–matrix interaction nearby the cracked surface is considered by estimating the amount of spalled matrix and by including local friction effects at the point where fiber exits the matrix. The approach embodies physical parameters and a formulation which is based on a set of key-points that govern the shape of the predictive multi-linear pullout diagram. Therefore an intuitive explanation on how material properties influence the several stages of pullout process is provided.

Comprehensive validation against experimental data highlight a good agreement on the load-crack width responses of fibers with different diameters, tensile strengths, embedded lengths and inclination angles within dissimilar matrix properties.

This model enables the prediction of the fundamental strengthening mechanisms existing on SFRC. This way, with a database of the pullout of aligned fibers, the performance of different fibers and matrices can be evaluated at any orientation. Given the random nature of fiber orientation in FRC applications, this means that material tailoring can be done in a much more realistic scenario.

Future research should be carried out to enlarge the scope of application of the present model on SFRC applications. For that purpose, factors that were not covered in this paper should be taken into account:

- Flexibility of the fiber (dependent on the type of steel, aspect ratio, etc.)
- Type of loading (e.g.: loading-rate, cyclic loading)
- Influence of neighboring fibers on the matrix spalling phenomenon.

The integration of the above aspects into the present model would allow an even more realistic quantification of each fiber's contribution to the composite strength.

Acknowledgment

The first author gratefully acknowledges the grant SFRH/BD/36248/2007 provided by the *Fundação para a Ciência e a Tecnologia* (FCT) from Portugal.

Appendix 1. Notations

P	= Pullout load (orthogonal to cracked surface)	[N]
δ	= Displacement along load direction	[mm]
w	= Crack width along load direction	[mm]
Δw	= Increment of crack width along load direction	[mm]
θ	= Fiber inclination angle relatively to load direction	[degrees]
d	= Diameter of fiber cross-section	[mm]
f_{cm}	= Average compressive strength of the cement matrix	[MPa]
f_{ctm}	= Average tensile strength of the cement matrix	[MPa]
μ	= Friction coefficient between steel fibers and cement matrix	[−]
L_e	= Shorter fiber embedded length within the cement matrix	[mm]
L_{SP1}	= Length of spalled matrix generated by P_{S01}	[mm]
L_{SP2}	= Increment of spalled matrix generated by P_{H01}	[mm]
$L_{eff\,(Hi)}$	= Effective fiber length factor at point H_i	[−]
$L_{H,crit}$	= Critical fiber embedded length	[mm]
S_i	= Key-point *i* governing the shape of the pullout diagram of straight fibers inclined relatively to the loading direction	[−]
S_{i0}	= Key-point *i* governing the shape of the pullout diagram of straight fibers aligned relatively to the loading direction	[−]
P_{Si}	= Pullout load at key-point S_i	[N]
P_{SAi}	= Component of the pullout load at key-point S_i derived from the direction of the original embedded part of the fiber	[N]
P_{SN}	= Non-aligned component of the pullout load	[N]
w_{Si}	= Crack width at key-point S_i	[mm]
w_{SAi}	= Component of the crack width at key-point S_i derived from the direction of the original embedded part of the fiber.	[mm]
w_{SNi}	= Component of the crack width at key-point S_i derived from the direction orthogonal to the original embedded part of the fiber	[mm]
Δw_{SP1}	= Increment of crack width due to matrix spalled length L_{SP1}	[mm]
Δw_{SP2}	= Increment of crack width due to matrix spalled length L_{SP2}	[mm]
H_i	= Key-point *i* governing the shape of the pullout diagram of hooked fibers inclined relatively to the loading direction	[−]
H_{i0}	= Key-point *i* governing the shape of the pullout diagram of hooked fibers aligned relatively to the loading direction	[−]
P_{Hi}	= Pullout load at key-point H_i	[N]
P_{HAi}	= Component of the pullout load at key-point H_i derived from the direction of the original embedded part of the fiber	[N]
P_{HN}	= Component of the pullout load derived from the direction orthogonal to the original embedded part of the fiber	[N]
w_{Hi}	= Crack width at key-point H_i	[mm]
w_{HAi}	= Component of the crack width at key-point H_i derived from the direction of the original embedded part of the fiber.	[mm]
w_{HNi}	= Component of the crack width at key-point H_i derived from the direction orthogonal to the original embedded part of the fiber	[mm]
Δw_{H0i}	= Increment of crack width during the stage *i* of the straightening process of the hook	[mm]
ΔP_{H0i}	= Increment of pullout load during the stage I of the straightening process of the hook	[N]
D_{F1}	= Deviation force at fiber exit point generated by P_{S01}	[N]
D_{F2}	= Deviation force at fiber exit point generated by P_{H01}	[N]
F_{SP1}	= Component of D_{F1} which generates matrix spalled length L_{SP1}	[N]
F_{SP2}	= Component of D_{F2} which generates matrix spalled length L_{SP2}	[N]
A_{SP2}	= Surface failure of the wedge of spalled matrix with length L_{SP2}	[mm^2]
a_1	= Second order term of the quadratic function used to obtain L_{SP1}	[−]
b_1	= First order term of the quadratic function used to obtain L_{SP1}	[mm]
c_1	= Constant term of the quadratic function used to obtain L_{SP1}	[mm^2]
a_2	= Second order term of the quadratic function used to obtain L_{SP2}	[−]
b_2	= First order term of the quadratic function used to obtain L_{SP2}	[mm]
c_2	= Constant term of the quadratic function used to obtain L_{SP2}	[mm^2]
G_1	= End section of the fiber hooked-end	[−]
G_2	= Intermediate section of the fiber hooked-end closer to G_1	[−]
G_3	= Intermediate section of the fiber hooked-end distant from G_1	[−]
σ_y	= Average tensile yield strength of aligned steel fibers	[MPa]
σ_u	= Ultimate tensile strength of aligned steel fibers	[MPa]
$\sigma_u(\theta)$	= Ultimate tensile strength of inclined steel fibers at angle θ	[MPa]
P_u	= Average ultimate pullout load of aligned steel fibers	[N]
$P_u(\theta)$	= Average ultimate pullout load of inclined steel fibers at angle θ	[N]
E_f	= Elastic modulus of the steel fibers	[MPa]
ε_u	= Ultimate strain of the steel fibers	[‰]
ε_a	= Strain of the steel fibers due to axial loading	[‰]
ε_c	= Strain of the steel fibers due to curvature at fiber exit point	[‰]
$\Delta\varepsilon_p$	= Plastic strain range of the steel fibers constitutive diagram	[‰]
R_F	= Idealized fiber radius of curvature at failure	[mm]
R_P	= Component of R_F due to steel yielding	[mm]
R_C	= Component of R_F due to curvature at fiber exit point	[mm]
k	= Parameter taking into account the pullout test configuration	[−]
N	= Number of sides of the cracked at which spalling of the matrix occurs	[−]

Appendix 2. Definition of L_{SP2}

Following the methodology adopted in [14], the increment of spalled matrix along fiber axis (L_{SP2}) is calculated through a failure criterion between the new spalling force (F_{SP2}) and the resisting mechanism provided by the matrix wedge (R_{SP2}). Likewise L_{SP2} represents the increment of spalled length at which the second stage of matrix spalling ceases, obtained by Eq. (A2.1).

$$R_{SP2} \geq F_{SP2} \tag{A2.1}$$

The resisting mechanism provided by the matrix (R_{SP2}) is a very complex one, with tensile and shear stresses generating non-uniform and brittle failure surfaces. This approach assumes that the tensile strength of the matrix (f_{ctm}) is the major and unique parameter controlling resistance against spalling and that the tensile strength is attained uniformly over the failure surface, thus being defined by:

$$R_{SP2} = A_{SP2} f_{ctm} \tag{A2.2}$$

Where A_{SP2} is the surface failure of the matrix wedge, defined in Eqs. (A2.3)–(A2.5) and depicted in Fig. A2.1.

$$A_{SP2} = A_{SP2,1} + A_{SP2,2} \tag{A2.3}$$

$$A_{SP2,1} = (L_{SP1} + L_{SP2}) \frac{\cos\theta}{\sin\theta} \left[d + (L_{SP1} + L_{SP2}) \frac{\cos\theta}{\sin\theta} \right] \tag{A2.4}$$

$$A_{SP2,2} = L_{SP2} \sqrt{2} \frac{\cos\theta}{\sin\theta} (2L_{SP1} + L_{SP2}) \tag{A2.5}$$

Due to the increment of load carrying capacity provided by the hook an increased deviation force arises at the new fiber exit point, leading to the spalling force defined in Eq. (A2.6).

$$F_{SP2} = P_{H01} \sin\theta \cos\theta \tag{A2.6}$$

The increment of matrix spalled length (L_{SP2}) can then be calculated by solving a quadratic function $a.L_{SP2}^2 + b.L_{SP2} + c = 0$ with the following parameters:

$$a_2 = a_1 \tag{A2.7}$$

$$b_2 = b_1 + \frac{2L_{SP1}\left(\cos\theta + \sqrt{2}\right)}{\sin\theta} \tag{A2.8}$$

$$c_2 = c_1 \frac{P_{H01}}{P_{S01}} + \frac{L_{SP1}}{\sin\theta}\left(d + L_{SP1}\frac{\cos\theta}{\sin\theta}\right) \tag{A2.9}$$

Where a_1, b_1 and c_1 are the parameters of the analogous quadratic function used to calculate L_{SP1} [14].

Appendix 3. Predicting $\sigma_u(\theta)$

In the following, the inclined tensile strength of steel fibers is taken as the ratio between the ultimate pullout load of an inclined fiber and its respective cross-sectional area. This way, it is not a material

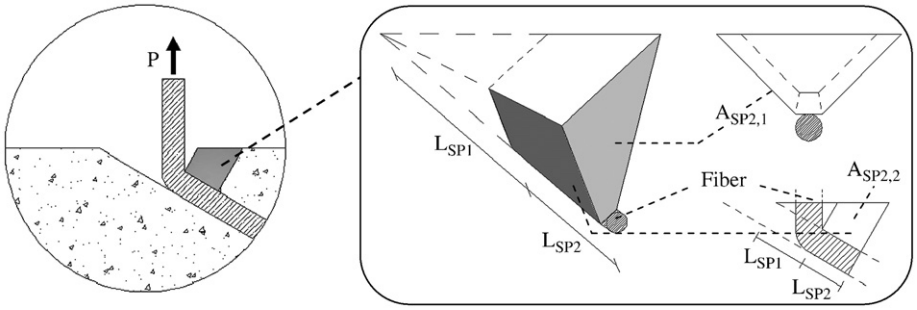

Fig. A2.1. Geometry of the matrix wedge at the second stage of spalling.

property but rather a parameter that comprises all together tensile, shear and bending stresses.

To include $\sigma_u(\theta)$ within the current approach a simplified heuristic procedure has been adopted. Firstly an inspection on the ultimate loads of steel fibers with different tensile strengths and pulled out at different inclination angles was performed to identify the magnitude and variations of the ultimate loads. For such purpose the experimental works on fibers with circular cross-sections [5,10,11] were taken into account to evaluate the dependency of $\sigma_u(\theta)$ with the inclination angles, fiber diameters, tensile strengths and testing configurations, such as shown in Table A3.1.

The reduction of the ultimate loads at increasing inclination angles is clearly denoted in Table A3.1, whose values were reported with maximum coefficients of variation of about 5%. Such reduced scattering is of the same magnitude of the one observed in the aligned case, denoting a unique dependency on the properties of the fiber itself.

The main properties of commercial steel fibers currently in the market and used on previous research works were investigated and their typical properties are summarized in Table A3.2. Regarding such values an elastoplastic constitutive diagram for the tensile behavior of steel fibers can be idealized (Fig. A3.1). For simplicity the plastic range of the diagram ($\Delta\varepsilon_p$) is assumed to be constant and to comprehend two components, namely axial strain (ε_a) and fiber curvature (ε_c).

The radius of curvature of the fiber at failure (R_F) can then be idealized as an upper bound value due to material yielding (R_P) and a reduction component to account for the actual curvature at fiber exit point (R_C):

$$R_F = R_P - R_C\theta \tag{A3.1}$$

The first component of R_F is obtained through the aligned case (Eq. (A3.2)). The decrease in the radius of curvature with the inclination angle shall include the influence of fiber diameter and tensile strength. Furthermore it shall also consider the effect of testing configuration, regarding that single-sided pullout tests on inclined fibers require bending the fibers prior to testing, which tends to reduce the ultimate pullout loads. Therefore, according to the experimental data presented in Table A3.1, an empirical expression for R_C is proposed in Eq. (A3.3).

$$R_P = \frac{d}{2\left(\frac{\varepsilon_u}{1000} - \frac{\sigma_u}{E_f}\right)} \tag{A3.2}$$

$$R_C = kd\sigma_u 10^{-6} \tag{A3.3}$$

With k being the parameter taking into account the pullout testing configuration, defined as following:

$$k = \begin{cases} 9 & \textit{if fiber geometry is the original one prior to testing} \\ 18 & \textit{if fiber is artificially deformed prior to testing} \end{cases} \tag{A3.4}$$

Taking into account Eqs. (A3.1)–(A3.4) the inclined tensile strength of the steel fibers can then be approximated by Eq. (A3.5):

$$\sigma_u(\theta) = E_f\left(\frac{\varepsilon_u}{1000} - \frac{d}{2R_F}\right) \tag{A3.5}$$

The ratios between the ultimate and co-axial tensile strengths at different inclination angles that arise from the application of this heuristic approach to common fiber properties are shown in Fig. A3.2. These results were obtained considering the data from Table A3.2 and pullout conditions similar to the ones existing in practice ($k=9$). Fig. A3.2 shows that the reduction of the ultimate tensile strengths at increasing inclination angles is not negligible and is particularly important for fibers with smaller tensile yield strengths.

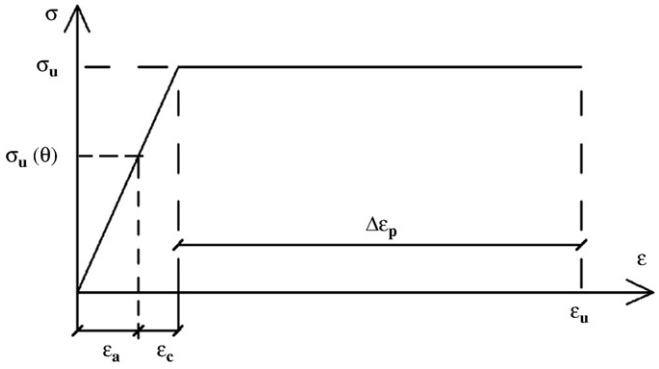

Fig. A3.1. Assumed constitutive diagram for tensile behavior of steel fibers.

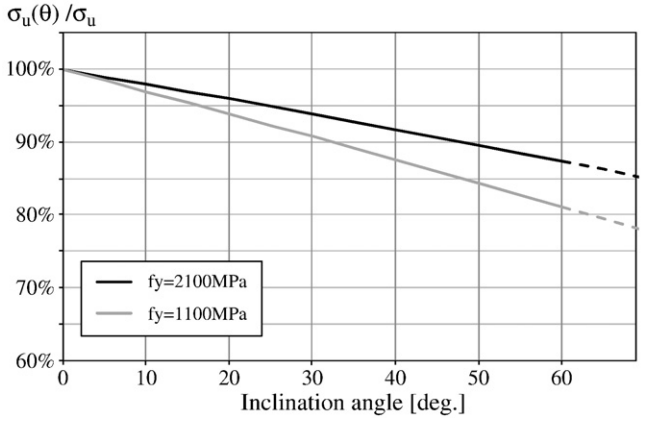

Fig. A3.2. Ratio between co-axial and inclined tensile strengths at different inclination angles.

It should be pointed out that this procedure is an approximation only valid for typical steel fibers and matrix properties such as the ones presented in Table A3.1, on fibers with circular cross-sections and with steel properties accordingly with Table A3.2. It is the author's opinion that, in the absence of improved predictive models, the inclined tensile strength shall be provided by the fibers' producers. In such scenario steel fibers should be tested under different inclination angles and without embedment on the matrix, according to the recommendations of other researchers [16]. This way, given that matrix spalling relieves bending stresses due to decreasing curvatures at fiber exit points, this data would provide lower bound values for the ultimate tensile strength of inclined fibers.

Table A3.1
Ratios of ultimate inclined pullout loads respect to aligned ones at different angles.

Reference	d [mm]	σ_u [MPa]	N	θ [deg.]		
				30	45	60
Van Gysel [5]	0,50	2148	1		86%	81%
Armelin and Banthia [10]	0,50	1150	2		86%	80%
Cunha et al. [11]	0,75	1141	1	83%		72%
Van Gysel [5]	0,80	2117	1		80%	79%

Table A3.2
Typical properties of steel fibers.

Fiber elastic modulus (E_f)	200 GPa
Tensile yield strength (σ_y)	1100/2100 MPa
Ultimate tensile strength (σ_u)	(1.05 to 1.10) σ_y
Ultimate strain (ε_u)	35‰

Appendix 4. Input values used for model validation

Table A4.1
Input values used for model validation.

Reference		Robins et al. [4]				Van Gysel [5]	
L_e	[mm]	20	15	10	5	30	30
d	[mm]	0.50				0.50	0.80
σ_u	[MPa]	1150				2148	2117
f_{ctm}	[MPa]	4.46				4.57	
N	[−]	2				1	
k	[−]	9				18	
μ	[−]	0.6				0.6	
P_{S01}	[N]	25.0				105.0	203.0
w_{S01}	[mm]	0.035				0.104	0.134
P_{S02}	[N]	12.5				52.5	101.5
w_{S02}	[mm]	0.3				0.3	0.3
P_{H01}	[N]	192.0	183.6	175.0	66.9	321.2	743.9
w_{H01}	[mm]	0.769	0.800	0.600	0.590	0.965	0.853
P_{H02}	[N]	110	110	105	0	200	550
w_{H02}	[mm]	2.6	2.0	2.3	3.0	2.2	1.9
P_{H03}	[N]	90	110	90	0	170	550
w_{H03}	[mm]	4.5	3.5	4.0	3.0	3.5	3.8
P_{H04}	[N]	65	60	55	0	130	350
w_{H04}	[mm]	5.0	4.5	5.0	3.0	5.0	4.5

References

[1] A.E. Naaman, Engineered steel fibers with optimal properties for reinforcement of cement composites, J. Adv. Concr. Technol. 1 (3) (2003) 241–252.
[2] N. Banthia, J. Trottier, Concrete reinforced with deformed steel fibers, Part I: bond-slip mechanisms, ACI Mater. J. 91 (5) (1994) 435–446.
[3] A.E. Naaman, H. Najm, Bond-slip mechanisms of steel fibers in concrete, ACI Mater. J. 88 (2) (1991) 135–145.
[4] P. Robins, S. Austin, P. Jones, Pull-out behavior of hooked steel fibres, Mater. Struct. 35 (2002) 434–442.
[5] Van Gysel, A. (2000) Studie van het uittrekgedrag van staalvezels ingebed in een cementgebonden matrix met toepassing op staalvezelbeton onderworpen aan buiging, PhD Thesis, Gent University.
[6] G. Chanvillard, Modeling the pullout of wire-drawn steel fibers, Cement Concr. Res. 29 (1999) 1027–1037.
[7] J.M. Alwan, A.E. Naaman, P. Guerrero, Effect of mechanical clamping on the pull-out response of hooked steel fibers embedded in cementitious matrices, Concr. Sci. Eng. 1 (1999) 15–25.
[8] C. Sujivorakul, A.M. Waas, A.E. Naaman, Pullout response of a smooth fiber with an end anchorage, J. Eng. Mech. 126 (9) (2000) 986–993.
[9] A.E. Naaman, G. Namur, J.M. Alwan, H.S. Najm, Fiber pullout and bond slip, I: Anal. Study J.Struct. Eng. 1 (9) (1991) 2769–2790.
[10] H. Armelin, N. Banthia, Predicting the flexural postcracking performance of steel fiber reinforced concrete from the pullout of single fibers, ACI Mater. J. 94 (1) (1997) 18–31.
[11] V.M.C.F. Cunha, J.A.O. Barros, J.S. Cruz, Pullout behaviour of hooked-end steel fibres in self-compacting concrete: report 07-DC/E06, Universidade do Minho, Guimarães, 2007.
[12] L. Prudencio Jr, S. Austin, P. Jones, H. Armelin, P. Robins, Prediction of steel fibre reinforced concrete under flexure from an inferred fibre pull-out response, Mater. Struct. 39 (2006) 601–610.
[13] L. Taerwe, A. Van Gysel, Influence of steel fibres on the design stress–strain curve for high-strength concrete, ASCE J. Eng. Mech. 122 (8) (1996) 695–704.
[14] F. Laranjeira, A. Aguado, C. Molins, Predicting the pullout response of inclined straight steel fibers, Journal of Materials and Structures 43 (6) (2010) 875–895 doi:10.1617/s11527-009-9553-4.
[15] A. Pompo, P.R. Stupak, L. Nicolais, B. Marchese, Analysis of steel fibre pull-out from a cement matrix using video photography, Cement Concr. Compos. 18 (1996) 3–8.
[16] P.J.M. Bartos, M. Duris, Inclined tensile strength of steel fibres in a cement-based composite, Composites 25 (10) (1994) 945–952.
[17] I. Markovic, J.G.M. Van Mier, J.C. Walraven, Experimental evaluation of fibre pullout from plain and fibre reinforced concrete, 4th International Workshop on HPFRCC, Ann Arbor, 2003, pp. 419–436.
[18] Duris (1993) Micromechanics of fracture of inclined fibres in a cement-based composite, PhD Thesis, University of West Scotland (formerlmy University of Paisley), 252pp.
[19] T.C. Easley, K.T. Faber, S.P. Shah, Use of a crack-bridging single fiber pullout test to study steel fiber/cementitious matrix composites, J. Am. Soc. 82 (12) (1999) 3513–3520.